References

[1] Valente, S.T. and Goff, S.P. (2006) Inhibition of HIV-1 gene expression by a fragment of hnRNP U. Mol. Cell 23, 597–605.

[2] Brass, A.L., Dykxhoorn, D.M., Benita, Y., Yan, N., Engelman, A., Xavier, R.J., Lieberman, J. and Elledge, S.J. (2008) Identification of host proteins required for HIV infection through a functional genomic screen. Science 319, 921–926.

[3] Komano, J., Miyauchi, K., Matsuda, Z. and Yamamoto, N. (2004) Inhibiting the Arp2/3 complex limits infection of both intracellular mature vaccinia virus and primate lentiviruses. Mol. Biol. Cell 15, 5197–5207.

[4] Shimizu, S. et al. (2007) Inhibiting lentiviral replication by HEXIM1, a cellular negative regulator of the CDK9/cyclin T complex. AIDS 21, 575–582.

[5] Kawano, Y., Yoshida, T., Hieda, K., Aoki, J., Miyoshi, H. and Koyanagi, Y. (2004) A lentiviral cDNA library employing lambda recombination used to clone an inhibitor of human immunodeficiency virus type 1-induced cell death. J. Virol. 78, 11352–11359.

[6] Biglione, S., Byers, S.A., Price, J.P., Nguyen, V.T., Bensaude, O., Price, D.H. and Maury, W. (2007) Inhibition of HIV-1 replication by P-TEFb inhibitors DRB, seliciclib and flavopiridol correlates with release of free P-TEFb from the large, inactive form of the complex. Retrovirology 4, 47.

[7] Jang, M., Mochizuki, K., Zhou, M., Jeong, H., Brady, J. and Ozato, K. (2005) The bromodomain protein Brd4 is a positive regulatory component of P-TEFb and stimulates RNA polymerase II-dependent transcription. Mol. Cell 19, 523–534.

[8] Yang, Z., Yik, J., Chen, R., He, N., Jang, M., Ozato, K. and Zhou, Q. (2005) Recruitment of P-TEFb for stimulation of transcriptional elongation by the bromodomain protein Brd4. Mol. Cell 19, 535–545.

[9] Bisgrove, D.A., Mahmoudi, T., Henklein, P. and Verdin, E. (2007) Conserved P-TEFb-interacting domain of BRD4 inhibits HIV transcription. Proc. Natl. Acad. Sci. USA 104, 13690–13695.

[10] Urano, E. et al. (2008) Cyclin K/CPR4 inhibits primate lentiviral replication by inactivating Tat/positive transcription elongation factor b-dependent long terminal repeat transcription. AIDS 22, 1081–1083.

[11] Salerno, D., Hasham, M.G., Marshall, R., Garriga, J., Tsygankov, A.Y. and Grana, X. (2007) Direct inhibition of CDK9 blocks HIV-1 replication without preventing T-cell activation in primary human peripheral blood lymphocytes. Gene 405, 65–78.

ELSEVIER

INSTITUT PASTEUR

Microbes and Infection 10 (2008) 1514–1523

www.elsevier.com/locate/micinf

Original article

Primary target cells of herpes simplex virus type 1 in the hippocampus

Yoshinori Ando [a,b], Hiroko Kitayama [a], Yasushi Kawaguchi [c], Yoshio Koyanagi [a,*]

[a] *Laboratory of Viral Pathogenesis, Institute for Virus Research, Kyoto University, 53 Shogoin-kawara-cho, Sakyo-ku, Kyoto 606-8507, Japan*
[b] *Department of Molecular and Cellular Biology, Graduate School of Biostudies, Kyoto University, Yoshida-konoe-cho, Sakyo-ku, Kyoto 606-8501, Japan*
[c] *Division of Viral Infection, Department of Infectious Disease Control, International Research Center for Infectious Diseases, The Institute of Medical Science, The University of Tokyo, 4-6-1 Shirokanedai, Minato-ku, Tokyo 108-8639, Japan*

Received 24 April 2008; accepted 3 September 2008
Available online 25 September 2008

Abstract

Herpes simplex virus type 1 (HSV-1) causes fatal and sporadic encephalitis in human. The encephalitis-survivors frequently suffer from symptoms of memory deficits. It remains unclear how HSV-1 induces tissue damages in memory formation-associated brain tissues such as the hippocampus. In this study, we examined HSV-1 infection in the hippocampus using a rat HSV-1 infection model. We found profound pathological changes in the hippocampus and large numbers of HSV-1 antigen-positive cells in the dentate gyrus (DG) subfield of HSV-1-infected rats. To understand the precise mechanism of HSV-1-induced tissue damages in the hippocampus, we employed rat organotypic hippocampal slice cultures (OHC) as an in vitro HSV-1 infection model. In OHC, HSV-1 infection predominated in neuronal cells and the infected neuronal cells were severely damaged. Longitudinal analysis indicated that granule cells in DG subfield were extremely vulnerable to HSV-1 infection among neuronal cells in the hippocampus. Since DG granule cells play a crucial role in memory formation, disruption of these cells may be a primary step leading to memory deficits.

Keywords: HSV-1; Hippocampus; Organotypic hippocampal slice cultures; Dentate gyrus; Neuron

1. Introduction

Herpes simplex virus (HSV) frequently invades the central nervous system (CNS) and induces severe encephalitis (HSV encephalitis, HSE) in human. HSE patients show several symptoms including fever, headache, mental abnormalities, seizure, and aphasia [1–5]. HSE survivors often suffer from neurological sequelae, most frequently, memory deficit [6]. Typical pathological changes in HSE are necrotization in medial temporal lobe and orbital surface of frontal lobe [5]. The amnestic impairments have been explained by the damages in medial temporal lobe [6]. Temporal lobe contains the limbic systems, including the hippocampus, the amygdala, the entorhinal and perirhinal cortex, that are critical for declarative anterograde memory [6]. It has been reported that HSV-1 antigen-positive cells are frequently found in these limbic regions of HSE patients [1,3,7].

The hippocampus tissue is highly vulnerable to anoxia, ischemia, and tissue damages caused by viruses such as human immunodeficiency virus 1 (HIV-1), borna disease virus (BDV), and HSV. In HIV-infected models, the hippocampus is damaged likely by viral and host factors released from HIV-1-infected macrophages [8,9]. In BDV-infected rats, selective neuronal cell degeneration occurs in the dentate gyrus (DG) [10].

In the present study, we examined the mechanism of HSV-1 infection in the hippocampus. Using organotypic hippocampal slice cultures (OHC), we found that HSV-1 primarily attacked neuronal cells but not glial cells. More importantly, among neuronal cells in the hippocampus, we found that granule cells in DG subfield were initially killed through HSV-1-mediated cytopathic effect, suggesting that DG granule cells were primary HSV-1 victims in the hippocampus.

* Corresponding author. Tel.: +81 75 751 4811; fax: +81 75 751 4812.
E-mail address: ykoyanag@virus.kyoto-u.ac.jp (Y. Koyanagi).

1286-4579/$ - see front matter © 2008 Elsevier Masson SAS. All rights reserved.
doi:10.1016/j.micinf.2008.09.005

2. Materials and methods

2.1. Cells and viruses

Vero cell line was maintained in Dulbecco's modified Eagle Medium supplemented with 10% fetal calf serum. A wild-type HSV-1, HSV-1 strain F [HSV-1 (F)] and a green fluorescent protein (GFP)-expressing replication-competent HSV-1 (YK333) [11], which is HSV-1 (F)-based and replicates in a similar manner with HSV-1 (F) in Vero cells, were propagated in Vero cells and the titers were determined by standard 50% tissue culture infective dose ($TCID_{50}$) on Vero cells.

2.2. HSV-1 infection in rats and tissue collection

Fourteen-day-old Wistar Hannover GALAS rats (CLEA Japan, Inc., Japan) were intranasally inoculated with 5×10^5 $TCID_{50}$ HSV-1 (F) or phosphate-buffered saline (PBS) [12]. When inoculated rats showed weakening with weight loss, trembling, paralysis, and/or seizure, the animals were sacrificed and brain tissues were collected. For histological examinations, samples were fixed by immersion in 4% paraformaldehyde, and then sectioned using a cryostat microtome and were stained with hematoxylin and eosin (HE). The degree of tissue damages in brain tissues was classified into 4 groups and the percentage of the area displaying cell lost in the coronal section was shown as follows: −, <5%; +, 5–10%; ++, 10–30%; +++, >30%. To estimate neuronal cell loss in brain tissues, neuronal nuclei (NeuN) were immunostained and the intensity was quantified using Image J software. Data were normalized with that in PBS-inoculated rat. The degree of neuronal cell loss was shown as NeuN intensity ratio and was classified into 4 groups: +++, <0.3; ++, 0.3–0.5; +, 0.5–0.9; −, >0.9. All animal experiments were carried out according to the guidelines for animal experimentation at the Kyoto University.

2.3. Organotypic hippocampal slice cultures and HSV-1 infection

OHC were prepared from postnatal day 7–8 Wistar Hannover GALAS rats (CLEA Japan, Inc.) as previously described [9,13]. Two weeks after initiation of culture, slice cultures were cocultured with HSV-1-infected Vero cells. The Vero cells were infected on the previous day at multiplicity of infection of 1. Twelve hours after cocultivation, the slices were transferred to fresh medium and cultured. HSV-1 titers in the slices were measured by standard $TCID_{50}$ method after the slices were homogenized. For inhibition of HSV-1, we added 25 μg/ml of acyclovir (Sigma-Aldrich, St. Louis, MO, USA) in culture medium.

2.4. PCR

Polymerase chain reaction (PCR) was carried out using AmpliTaq Gold (Applied Biosystems Japan, Ltd., Japan) according to the manufacturer's protocol. One hundred nanogram of sample DNA was used. PCR product of HSV-1 glycoprotein B (gB) and glyceraldehyde-3-phosphate dehydrogenase (GAPDH) were obtained after amplification for 35 and 30 cycles, respectively. Specific primer pairs against HSV-1 gB and GAPDH are as follows: gB-F, 5′-TCGCCTTTCGCTACGTCAT-3′; gB-R, 5′-GGTTCTTGA GCTCCTTGGTGG-3′; GAPDH-F, 5′-ACTAAAGGGCATC CTGGGCTA-3′; GAPDH-R, 5′-TGGAAGAATGGGAGTTG CTGT-3′.

2.5. Antibodies

The following antibodies were used: anti-HSV and anti-glial fibrillary acidic protein (GFAP) rabbit polyclonal antibodies (DakoCytomation, Carpinteria, CA, USA); anti-HSV-1 ICP27 and anti-HSV-1 gB goat polyclonal antibodies (Santa Cruz Biotechnology, Inc., Santa Cruz, CA, USA); anti-HSV-1 ICP5 mouse monoclonal antibody (clone 3B6, Virusys Corporation, Sykesville, MD, USA); anti-NeuN mouse monoclonal antibody (clone A60, Chemicon International, Inc., Temecula, CA, USA); Alexa Fluor 488-conjugated goat anti-mouse and Alexa Fluor 594-conjugated goat anti-rabbit IgG (Invitrogen, Carlsbad, CA, USA); fluorescein isothiocyanate (FITC)-conjugated donkey anti-goat IgG (Chemicon International, Inc.).

2.6. Immunohistochemistry

Rat brain sections were permeabilized with 0.1% Triton X-100, then were incubated with blocking buffer containing 5% normal goat serum (Vector Laboratories, Inc., Burlingame, CA, USA), followed by incubation with primary antibodies. Samples were subsequently incubated with secondary antibodies. Immunohistochemical (IHC) staining and examination of OHC were carried out as previously described [9]. Nuclei were stained using Hoechst33342 dye (Invitrogen).

2.7. Measurement of cell damage in OHC

Cellular uptake of propidium iodide (PI, Invitrogen) was used for the estimation of cell damage [14]. PI was added at 5 μg/ml and the cultures were incubated for 30 min at 34 °C. Nuclei were stained using Hoechst33342 dye (Invitrogen). Each sample was examined under a confocal laser microscope (TCS SP2 AOBS, Leica Microsystems, Heidelberg, Germany). The quantification of fluorescent intensity was done following the protocol supplied by manufacturer (LCS Lite software, Leica Microsystems).

2.8. Statistical analysis

Data were generated from at least three replicate experiments. Statistical analysis was carried out by one-way ANOVA. Multiple comparisons were performed with Student's t test. A P value of less than 0.05 was considered significant.

3. Results

3.1. HSV-1 induces neuronal cell loss in the hippocampus

We first studied the pathogenesis of HSE in rats intranasally inoculated with HSV-1 (F). A total of 9 rats were infected, and within 3 days post infection (dpi), all rats appeared healthy. However, among them, 8 rats (#1–8) showed severe weakening with weight loss, trembling, and the symptoms of severe encephalitis such as paralysis and/or seizures on 4 or 5 dpi. Although one rat of the infected group (#9) gained weight and had no neurological illness similar to PBS-inoculated rat prior to 7 dpi, after 7 dpi, body weight gradually decreased and it showed weakening with trembling and paralysis (Fig. 1A). We confirmed HSV-1 infection by PCR analysis using HSV-1 gB-specific primers. Tissue damages were evaluated by histological examination in brain tissues, although tissue samples from some of the infected rats (#4, #6, and #8) were not available because of sudden deaths by severe encephalitis. As shown in Fig. 1B, HSV-1 gB DNA was detected by 4 dpi in the cerebral cortex, the hippocampus, the olfactory bulb, and the trigeminal ganglia of the infected rats but not in those of mock-infected (PBS-inoculated) rat (Fig. 1B). HE-stained brain sections from 4 to 10 dpi revealed tissue damages displaying focal hemorrhagic cell loss and cell infiltration in cerebral cortex, the hippocampus, and the medulla of the infected rats (Fig. 1C and Table 1). These data indicate that HSV-1 efficiently disseminates to the hippocampus as well as other brain tissues and induces hippocampal damages. Since it is well known that the hippocampus forms neuronal network and that this is essential for memory formation [15], we next examined neuronal cell loss in the hippocampus. Co-immunostaining for NeuN and HSV-1 in brain sections from 4 to 10 dpi indicated that the number of NeuN antigen-positive neuronal cells in the hippocampus of HSV-1-infected rats was severely reduced as similar to other regions of brain such as cerebral cortex and medulla (Fig. 1D a, b and Table 1), and large numbers of HSV-1 antigen-positive cells were found in the hippocampus (Fig. 1D a and c). Notably, many of HSV-1 antigen-positive cells were localized at DG subfield, suggesting that DG granule cells might be preferentially infected with HSV-1. Large numbers of HSV-1 antigen-positive cells were also found in other regions of brain (data not shown). These data indicate that HSV-1 infection induces severe neuronal cell loss at the hippocampus.

3.2. Longitudinal analysis of HSV-1 infection in the CNS using organotypic hippocampal slice cultures

Since animal models have limitations for longitudinal pathological analyses, we employed OHC. Physiological and morphological features of OHC closely resemble those of the actual hippocampus and would provide an alternative model to the hippocampus in vivo. As cellular composition and architecture within the hippocampus are well preserved in OHC, the main neuronal network organization is very similar to that of living animals [9,16]. However, unlike the bona fide hippocampus, in OHC, there are layers of glial cells above and below the main area containing neuronal cell layers [13]. For this reason, the slices were exposed to HSV-1 released from the infected Vero cells across the porous membrane to efficiently infect the neuronal cells and the glial cells that are immersed in slice cultures with HSV-1. To examine the precise mechanism of HSV-1-induced hippocampal damages in vitro, we first verified the longitudinal alteration of OHC by HSV-1 infection. We measured virus titers in the slices. As shown in Fig. 2A, the highest level of virus production was detected on 5 dpi and virus production was maintained for at least 10 days. After the slices were infected with HSV-1 (F), neuronal cell layers were gradually destroyed and their tissue architectures were largely disrupted by 10 dpi (Fig. 2B, top panels). To visualize longitudinal HSV-1 dissemination, we next used a GFP-expressing replication-competent HSV-1, HSV-1 (YK333). We confirmed that similar level of HSV-1 production took place in HSV-1 (YK333)-infected slices compared to that in HSV-1 (F)-infected slices (Fig. 2A). GFP-positive cells were initially detected in the borders of the slices at 3 dpi. Keeping with cultivation, HSV-1 (YK333) massively disseminated to entire slices by 5 dpi and then GFP expression was gradually reduced. In accordance with this, the tissue architectures of HSV-1 (YK333)-infected slices were gradually disrupted as were in HSV-1 (F)-infected slices (Fig. 2B, middle panels). In addition, we tested whether an anti-HSV drug, acyclovir, exhibited the capacity to inhibit HSV-1 replication in OHC. As shown to Fig. 2C, addition of acyclovir to the culture medium starting at 24 h prior to HSV-1 (YK333) infection remarkably inhibited HSV-1 dissemination in the slices, and their tissue architectures were also not affected (Fig. 2C, top panels). However, when acyclovir treatment was started on 3 dpi, HSV-1 could disseminate to entire slices and the tissue architectures of the slices were gradually destroyed as a similar manner to untreated slices (Fig. 2C, bottom panels). We also examined and confirmed with HSV-1 (F) (data not shown). From these longitudinal analyses, HSV-1 infection may have occurred in the neuronal cells and the glial cells on 5 dpi. To confirm this, viral proteins in HSV-1 (F)-infected slices were immunostained. In the infected slices on 1 and 3 dpi, viral proteins were expressed only in a part of the slices as similar to the results obtained using HSV-1 (YK333) (data not shown). In contrast, as shown in Fig. 2D, the viral proteins including ICP27, ICP5, and gB expressed throughout the slices on 5 dpi, and neuronal cell layers were clearly immunostained using anti-ICP5 antibody at this time point. Taken together, these results indicated that on 5 dpi, HSV-1 infection extensively disseminated in OHC and the neuronal cells were infected with HSV-1.

3.3. Primary disruption of neuronal cells in the hippocampus by HSV-1

To assess cellular damages caused by HSV-1 infection in the hippocampus, we immunostained the slices for NeuN (neuronal cell marker) and GFAP (astrocyte marker). As

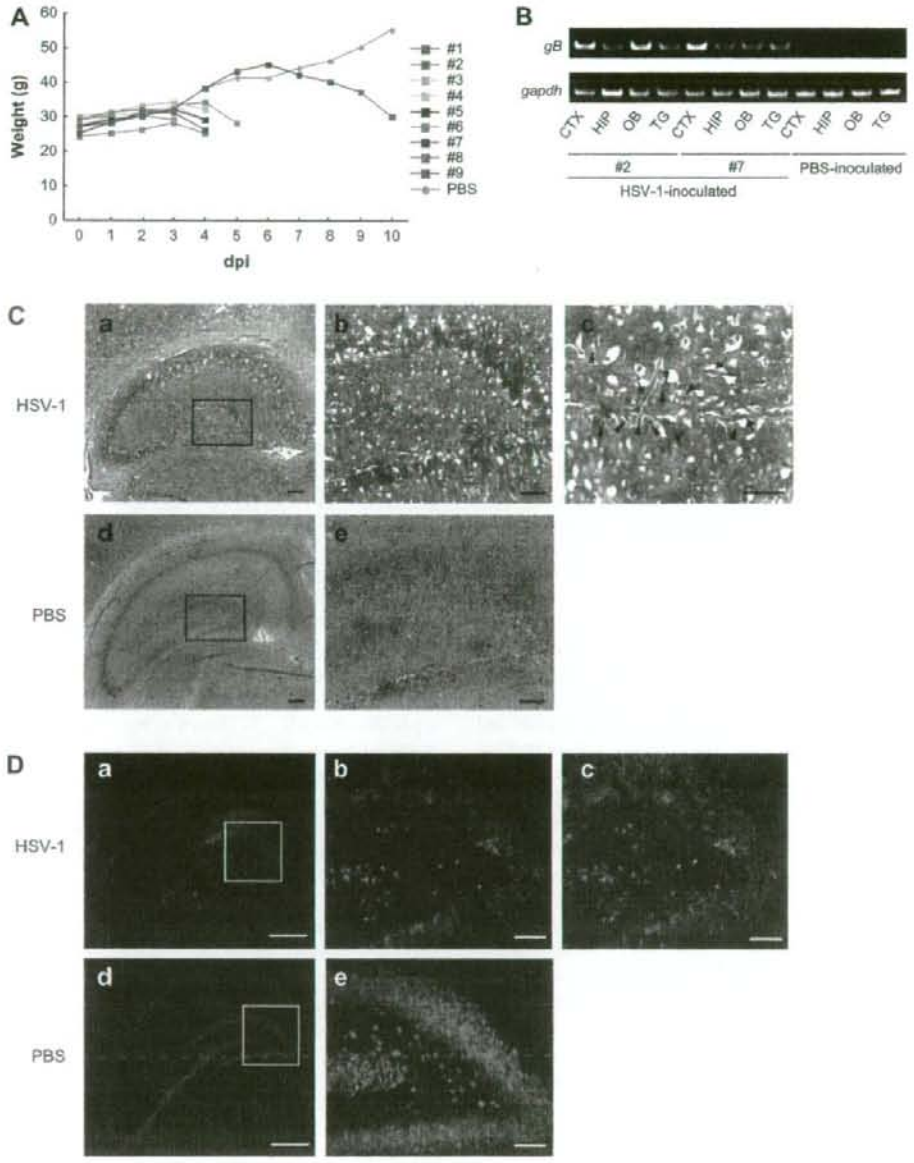

Fig. 1. Tissue damages in the hippocampus of HSV-1-infected rats. (A) Body weight of rats after HSV-1 inoculation. (B) PCR analysis using HSV-1 gB- and GAPDH-specific primers in total DNA extracted from the cerebral cortex (CTX), the hippocampus (HIP), the olfactory bulb (OB), and the trigeminal ganglia (TG). Representative results of two infected rats on 4 dpi and one PBS-inoculated rat are shown. (C) HE staining of the hippocampus in the infected rat on 10 dpi (a, b, c) or PBS-inoculated rat (d, e). Arrows indicate hemorrhagic lesions and arrowheads indicate cell infiltration. Rectangular regions in C-a and C-d are enlarged and shown in C-b and C-e, respectively. Scale bars show 300 μm (a, d), 100 μm (b, e), and 50 μm (c). (D) IHC examination for NeuN (green) and HSV-1 antigens (red) in the hippocampus of the infected rat on 10 dpi (a, b, c) or PBS-inoculated (d, e) rats. Rectangular regions in D-a and D-d are enlarged and shown in D-b, -c, and D-e, respectively. Scale bars show 500 μm (a, d) and 100 μm (b, c, e). Representative results are shown (C, D).

shown in Fig. 3, in the infected slices on 5 dpi, the numbers of NeuN antigen-expressing cells were significantly reduced, while the numbers of GFAP antigen-expressing cells were not affected. To ascertain these phenomena, we carried out IHC examination using antibodies against β-3-tubulin (B3T, neuronal cell marker), microtubule-associated protein 2 (MAP2, neuronal cell marker, expressed in cell bodies and dendrites), neurofilament protein (NFP, neuronal cell marker,

Table 1
HSV-1-induced tissue damages in the brain

Rat ID	HSV-1 inoculation	dpi	Hippocampus				Cerebral cortex				Medulla	
			Right		Left		Right		Left			
			Tissue damages[a]	Neuronal cell loss[b]	Tissue damages	Neuronal cell loss	Tissue damages	Neuronal cell loss	Tissue damages	Neuronal cell loss	Tissue damages	Neuronal cell loss
#1	+	5	+	+	+	++	+	+	+	++	+	++
#3	+	4	+	+	+	++	++	+	+	+	+	+
#5	+	4	+	+	+	++	+	+	+	+	+	+++
#9	+	10	+++	++	++	+++	++	++	++	++	++	+++
PBS	–	10	–	–	–	–	–	–	–	–	–	–

[a] The percentage of the damaged area in the coronal section is presented as follows: –, <5%; +, 5–10%; ++, 10–30%; +++, >30%.
[b] Using Image J software, NeuN intensity in the coronal section was quantified and data are shown as NeuN intensity of the brain tissue in each rat/that in PBS-inoculated rat ratio. The degree of neuronal cell loss is presented as follows: +++, <0.3; ++, 0.3–0.5; +, 0.5–0.9; –, >0.9.

expressed in axons), and S100b (astrocyte marker). Similar to Fig. 3, the numbers of B3T antigen-, MAP2 antigen-, or NFP antigen-positive neuronal cells were clearly reduced in the infected slices, while the numbers of S100b antigen-positive astrocytes in the infected slices were similar to that in uninfected slices on 5 dpi (data not shown). These results indicate that neuronal cells are more vulnerable to HSV-1-induced damages than glial cells.

Since HSV-1 is a neurotropic virus, we assumed that the vulnerability of neuronal cells to HSV-1 infection was associated with HSV-1 neurotropism. To ascertain this assumption, we carried out co-immunostaining for HSV-1 antigens and NeuN in the infected slices. We found abundant HSV-1 antigen-positive cells in CA1, CA3, and DG subfields (Fig. 4A). Identical to previous findings, NeuN antigen-positive neuronal cell layers were surrounded by GFAP antigen-positive cells [13], and NeuN expression was found in the dense clusters of nuclei [17]. It has been reported that the dense clusters of nuclei in the hippocampus correspond to neuronal cell layers [18]. In the infected slices, the dense clusters of nuclei were preserved, and were surrounded by GFAP antigen-positive cells as were in uninfected slices. However, NeuN expression was severely inhibited by HSV-1 infection (Fig. 3). In Fig. 4A, we found that large numbers of HSV-1 antigen-positive cells were located in the dense clusters of nuclei, indicating that HSV-1 infection mainly occurs in neuronal cells. Furthermore, to confirm this, we carried out co-immunostaining for ICP5 and GFAP. As shown in Fig. 4B, large numbers of ICP5 antigen-positive cells did not co-express GFAP, and they were located in the dense clusters of nuclei as similar to the results of immunostaining for HSV-1 antigens. This data indicated that HSV-1-infected and damaged cells were neuronal cells. Taken together, these results strongly suggest that HSV-1 preferentially infects neuronal cells and kills them faster than glial cells.

3.4. DG granule cells were the primary victims of HSV-1-induced tissue damages

In the hippocampus, there are 2 major classes of neuronal cells, which are pyramidal cells and granule cells. It was reported that HSV-1 antigens were frequently detected in granule cells residing in DG subfield of HSE patients [7]. To evaluate the population of neuronal cells infected with HSV-1 and to longitudinally analyze neuronal cell disruption, we used the PI uptake method and GFP-expressing HSV-1. Since this fluorescent dye rapidly intercalates into DNA of the necrotic cells losing plasma membrane integrity, we were able to detect HSV-1-induced necrosis [14]. Three days after infection with HSV-1 (YK333), we found few GFP-positive pyramidal cells in CA1 and CA3 subfields but large numbers of GFP-positive granule cells in DG subfield. At this time point, the numbers of GFP-positive cells in DG subfield were clearly larger than that in other subfields (Fig. 5A, top panels, $P < 0.05$ compared to CA1 and CA3 subfields), indicating that DG granule cells were more susceptible to HSV-1 infection than pyramidal cells. On 5 dpi, large numbers of pyramidal cells in CA1 and CA3 subfields and granule cells in DG subfield were found to be GFP positive. However, PI- and GFP-positive pyramidal cells in CA1 and CA3 subfields were a few, while numerous PI- and GFP-positive granule cells were detected in DG subfield. The numbers of PI-positive cells were also clearly higher in DG subfield (Fig. 5A, middle panels). By 10 dpi, the numbers of PI-positive cells increased in CA1, CA3, and DG subfields of the infected slices, and almost all granule cells in DG subfield became positive for PI (Fig. 5A, bottom panels). These results indicated that DG granule cells were more vulnerable to HSV-1 infection than pyramidal cells. We also examined and confirmed this with HSV-1 (F) (Fig. 5B). Taken together, these data suggest that in the hippocampus, granule cells in DG subfield are highly vulnerable to HSV-1 infection and are the primary victims of HSV-1-induced tissue damages.

4. Discussion

The mortality rate of HSE has been significantly improved because of the development of effective anti-HSV drugs. However, HSE frequently leaves its survivors with memory deficits [6]. This is due to the impairments in memory formation-associated brain tissues and it is well known that the hippocampus plays an important role for storage and recalling of information [6,15]. Although a variety of reports have been

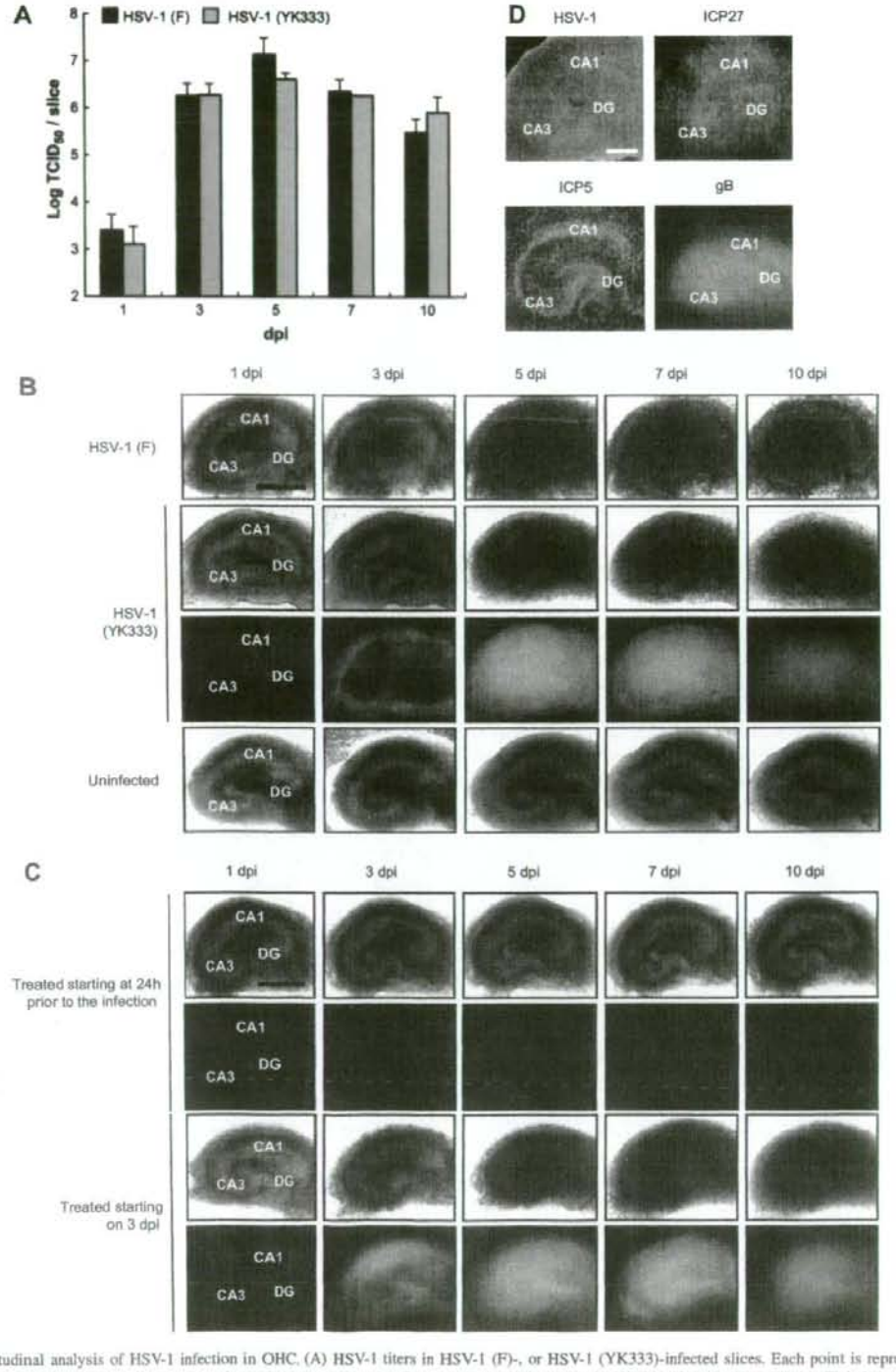

Fig. 2. Longitudinal analysis of HSV-1 infection in OHC. (A) HSV-1 titers in HSV-1 (F)-, or HSV-1 (YK333)-infected slices. Each point is represented as log $TCID_{50}$/slice ± SEM of virus titers from three independent experiments. (B) Longitudinal alterations in HSV-1-infected slices. HSV-1 (F)-infected (top panels), HSV-1 (YK333)-infected (middle panels), and uninfected (bottom panels) slices were observed up to 10 dpi. Scale bars show 1 mm. (C) Inhibition of HSV-1 replication in HSV-1 (YK333)-infected slices by acyclovir. Acyclovir treatment was started at 24 h prior to HSV-1 infection (top panels) or on third day after the infection (bottom panels). Scale bars show 1 mm. (D) IHC examination using the indicated antibodies in HSV-1 (F)-infected slices on 5 dpi. Scale bars show 500 μm. Representative results are shown (B, C, D).

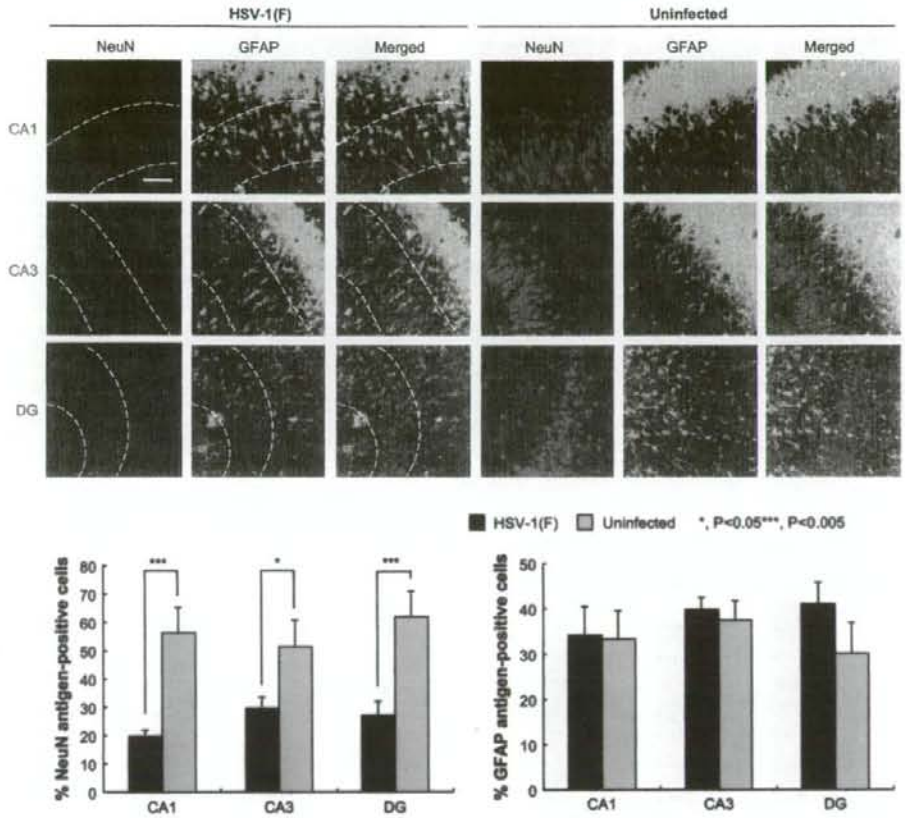

Fig. 3. Neuronal tissue damages in the hippocampus by HSV-1 infection. NeuN (red) and GFAP (green) in HSV-1 (F)-infected slices on 5 dpi or uninfected slices were co-immunostained and nuclei also were stained with Hoechst33342 (blue). The regions enclosed in the broken lines are neuronal cell layers. Scale bars show 75 μm. Representative results are shown. Quantification data were presented as the percentage of NeuN antigen-, or GFAP antigen-positive cells in Hoechst33342-stained nuclei ± SEM from three independent experiments. *, $P < 0.05$, ***, $P < 0.005$ compared to uninfected slices.

published on HSE experimental models and some have shown that HSV-1-infected mice display deficits in spatial recognition memory [19,20], the mechanism of HSV-1-induced tissue damages at the hippocampus is largely under examined. Therefore, we examined the longitudinal alteration of the hippocampus during HSV-1 infection in order to uncover the precise mechanism of hippocampal disruption.

We verified the involvement of the hippocampus in HSV-1 infection using rats intranasally inoculated with HSV-1. Our infected rats showed severe weakening with weight loss and typical clinical signs of neurological disorders (Fig. 1A). HSV-1 DNA was detected in various brain tissues, indicating that HSV-1 actually infected brain tissues of the encephalitis displaying-rats (Fig. 1B). These results are consistent with previous findings in rodent models and in humans [1,3,21]. It is known from pathological analysis of HSE autopsy samples that neuronal cells and glial cells are killed by HSV-1-induced necrosis [1,3,22]. HE-stained brain sections of our infected rats displayed focal hemorrhagic lesions and cell infiltration as well as severe cell loss in the hippocampus (Fig. 1C and Table 1). This suggests that the hippocampus of the infected rats was also mainly damaged via necrosis. In addition, Fig. 1D and Table 1 indicated that neuronal cells were severely reduced in number and that large number of HSV-1 antigen-positive cells was present in the hippocampus. These data indicate that the hippocampus is a major target tissue by HSV-1 infection.

To understand the mechanism of hippocampus disruption by HSV-1 infection, we need to carry out longitudinal evaluation of hippocampus tissue damages. However, animal models are not suitable for longitudinal analyses, especially for the investigations at the cellular level. Therefore, we used OHC. Neuronal cells and glial cells in OHC are thought to be within an microenvironment similar to that of the hippocampus in living animals [16]. Moreover, OHC has been used to elucidate some viral neuropathogenesis such as BDV and HIV-1 [9,10].

Firstly, we ascertained that HSV-1 efficiently induced tissue damages in OHC. After HSV-1 infection, the slices efficiently

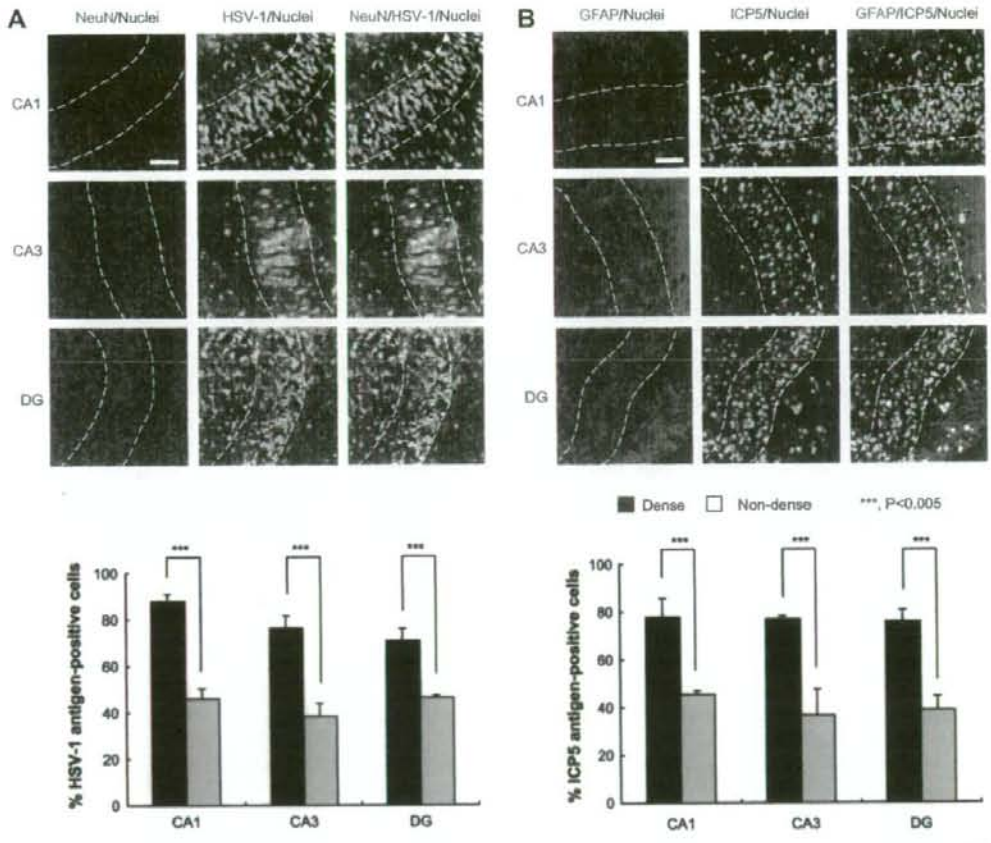

Fig. 4. HSV-1-infected cells in the hippocampus. (A) Co-immunostaining for NeuN (red) and HSV-1 antigens (green) in HSV-1 (F)-infected slices on 5 dpi. (B) Co-immunostaining for GFAP (red) and ICP5 (green) in HSV-1 (F)-infected slices on 5 dpi. Nuclei were also stained with Hoechst33342 (blue). The regions enclosed in the broken lines are the dense clusters of nuclei that indicate neuronal cell layers. Scale bars show 75 μm. Representative results are shown. Quantification data were presented as the percentage of HSV-1 antigen-, or ICP5 antigen-positive cells in Hoechst33342-stained nuclei ± SEM from three independent experiments. ***, $P < 0.005$ compared to the non-dense regions of nuclei.

released large numbers of infectious HSV-1 particles and expressed large amounts of HSV-1 proteins. As shown in Fig. 2B, HSV-1 promptly disseminated throughout the slices and the tissue architecture was gradually disrupted. Moreover, we found that HSV-1 disseminated throughout the slices on 5 dpi. These data indicate that we can evaluate HSV-1-induced hippocampal damages in vitro using OHC.

In animal models and humans, HSV-1 infection evokes immune responses such as humoral and cellular responses. After HSV-1 infection in vivo, humoral factors including complements, cytokines, and chemokines are released or activated, and macrophages, natural killer cells, dendritic cells, antigen-specific T cells, and B cells engage in the clearance of virions and virus-infected cells [23]. However, in OHC, the types of these immune cells and their numbers are limited, and consequently, virions as well as virus-infected cells would not be actively eliminated in the infected slices. As shown in Figs. 1D and 2B, there were differences in the distribution of HSV-1 antigen-positive cells between the hippocampus in vivo and the OHC. These may be explained by the differences in the presence of immune responses. OHC may have limitation of immune responses, but we think that by using OHC, we can understand the intrinsic differences in the sensitivity of hippocampal cells to HSV-1 infection.

An evaluation on cell damage by PI staining clearly demonstrated that granule cells in DG subfield were more vulnerable to HSV-1-induced damages than pyramidal cells in CA1 and CA3 subfields (Fig. 5). It has been reported that HSV-1 antigens were extensively detected in DG granule cells in autopsies of HSE patients [7], and that pronounced HSV-1 infection was observed in DG subfield of organotypic brain-slice cultures [24]. These data support our results obtained from experiments using OHC, and we concluded that DG granule cells were the primary victims of HSV-1-mediated

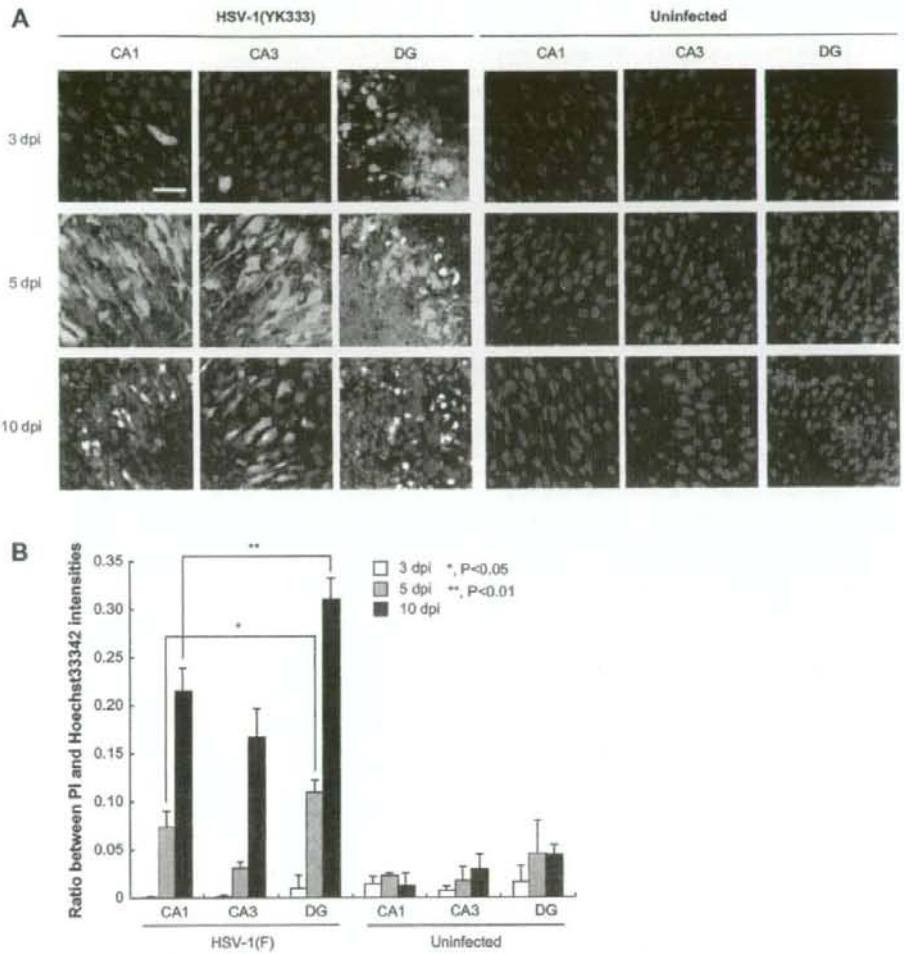

Fig. 5. Vulnerability of DG granule cells in the hippocampus. (A) Longitudinal analysis on HSV-1 (YK333)-infected slices. The infected (green) or uninfected slices were stained with PI (red) on 3, 5, and 10 dpi. Nuclei were also stained with Hoechst33342 (blue). Scale bar shows 40 μm. Representative results are shown. (B) Longitudinal analysis on HSV-1 (F)-infected slices. The infected or uninfected slices were stained with PI and Hoechst33342 on 3, 5, and 10 dpi. Using Leica software, PI intensity in each subfield was quantified. Data are presented as PI intensity/Hoechst33342 intensity ratio ± SEM from three independent experiments. *, $P < 0.05$, **, $P < 0.01$ compared to CA1 subfield of the infected slices.

cytopathic effect. Previous reports have indicated that BDV infection as well as humoral factors released from HIV-1-infected macrophages induced selective neuronal cell loss in DG granule cells [9,10,25]. Therefore, granule cells in DG subfield appear to be uniformly predisposed to virus-induced neurotoxic effects.

Acknowledgments

We thank Ms. Naoko Misawa and Mr. Chuanyi Nie for supports in our study.

This work was supported by a Grant-in-Aid for Scientific Research on Priority Areas from the Ministry of Education, Culture, Sports, Sciences, and Technology of Japan.

References

[1] R.J. Whitley, Herpes simplex encephalitis: adolescents and adults. Antiviral. Res. 71 (2006) 141–148.
[2] E. Schmutzhard, Viral infections of the CNS with special emphasis on herpes simplex infections, J. Neurol. 248 (2001) 469–477.
[3] P.G. Kennedy, A. Chaudhuri, Herpes simplex encephalitis, J. Neurol. Neurosurg. Psychiatr. 73 (2002) 237–238.
[4] P.G. Kennedy, Viral encephalitis, J. Neurol. 252 (2005) 268–272.

[5] D.H. Gilden, R. Mahalingam, R.J. Cohrs, K.L. Tyler, Herpesvirus infections of the nervous system, Nat. Clin. Pract. Neurol. 3 (2007) 82–94.
[6] L. Hokkanen, J. Launes, Cognitive outcome in acute sporadic encephalitis, Neuropsychol. Rev. 10 (2000) 151–167.
[7] M.M. Esiri, Herpes simplex encephalitis. An immunohistological study of the distribution of viral antigen within the brain, J. Neurol. Sci. 54 (1982) 209–226.
[8] R. Ellis, D. Langford, E. Masliah, HIV and antiretroviral therapy in the brain: neuronal injury and repair, Nat. Rev. Neurosci. 8 (2007) 33–44.
[9] H. Kitayama, Y. Miura, Y. Ando, Y. Koyanagi, Human immunodeficiency virus type-1 vulnerates nascent neuronal cells, Microbiol. Immunol. 52 (2008) 78–88.
[10] D. Mayer, H. Fischer, U. Schneider, B. Heimrich, M. Schwemmle, Borna disease virus replication in organotypic hippocampal slice cultures from rats results in selective damage of dentate granule cells, J. Virol. 79 (2005) 11716–11723.
[11] M. Tanaka, H. Kodaira, Y. Nishiyama, T. Sata, Y. Kawaguchi, Construction of recombinant herpes simplex virus type 1 expressing green fluorescent protein without loss of any viral genes, Microbes Infect 6 (2004) 485–493.
[12] S. Fujii, T. Akaike, H. Maeda, Role of nitric oxide in pathogenesis of herpes simplex virus encephalitis in rats, Virology 256 (1999) 203–212.
[13] M. Kamada, R.Y. Li, M. Hashimoto, M. Kakuda, H. Okada, Y. Koyanagi, T. Ishizuka, H. Yawo, Intrinsic and spontaneous neurogenesis in the postnatal slice culture of rat hippocampus, Eur. J. Neurosci. 20 (2004) 2499–2508.
[14] O. Chechneva, K. Dinkel, F. Cavaliere, M. Martinez-Sanchez, K.G. Reymann, Anti-inflammatory treatment in oxygen-glucose-deprived hippocampal slice cultures is neuroprotective and associated with reduced cell proliferation and intact neurogenesis, Neurobiol. Dis. 23 (2006) 247–259.
[15] G. Neves, S.F. Cooke, T.V. Bliss, Synaptic plasticity, memory and the hippocampus: a neural network approach to causality, Nat. Rev. Neurosci. 9 (2008) 65–75.
[16] B.H. Gahwiler, M. Capogna, D. Debanne, R.A. McKinney, S.M. Thompson, Organotypic slice cultures: a technique has come of age, Trends Neurosci. 20 (1997) 471–477.
[17] R.J. Mullen, C.R. Buck, A.M. Smith, NeuN, a neuronal specific nuclear protein in vertebrates, Development 116 (1992) 201–211.
[18] E. Forster, S. Zhao, M. Frotscher, Laminating the hippocampus, Nat. Rev. Neurosci. 7 (2006) 259–267.
[19] J.H. McLean, M.T. Shipley, D.I. Bernstein, D. Corbett, Selective lesions of neural pathways following viral inoculation of the olfactory bulb, Exp. Neurol. 122 (1993) 209–222.
[20] D.R. Beers, J.S. Henkel, R.P. Kesner, W.G. Stroop, Spatial recognition memory deficits without notable CNS pathology in rats following herpes simplex encephalitis, J. Neurol. Sci. 131 (1995) 119–127.
[21] Y. Becker, HSV-1 brain infection by the olfactory nerve route and virus latency and reactivation may cause learning and behavioral deficiencies and violence in children and adults: a point of view, Virus Genes 10 (1995) 217–226.
[22] L.E. Davis, R.T. Johnson, An explanation for the localization of herpes simplex encephalitis? Ann. Neurol. 5 (1979) 2–5.
[23] H. Wakimoto, P.R. Johnson, D.M. Knipe, E.A. Chiocca, Effects of innate immunity on herpes simplex virus and its ability to kill tumor cells, Gene Ther. 10 (2003) 983–990.
[24] E. Braun, T. Zimmerman, T.B. Hur, E. Reinhartz, Y. Fellig, A. Panet, I. Steiner, Neurotropism of herpes simplex virus type 1 in brain organ cultures, J. Gen. Virol. 87 (2006) 2827–2837.
[25] K.M. Carbone, S.W. Park, S.A. Rubin, R.W. Waltrip 2nd, G.B. Vogelsang, Borna disease: association with a maturation defect in the cellular immune response, J. Virol. 65 (1991) 6154–6164.

〔ウイルス　第58巻　第2号，pp.219-220，2008〕

トピックス

2. Sputnik Sweetheart – ウイルスに感染するウイルス

佐藤　佳，小柳義夫
京都大学ウイルス研究所ウイルス病態研究領域

新種の巨大ウイルス「ママウイルス」とそのサテライトウイルス「スプートニク」が，フランス・パリの冷却塔に生息するアメーバから発見された（La Scola et al, *Nature*, 2008）[4]．ママウイルスに寄生するような複製スタイルをとるスプートニクの発見は，これまでのウイルスの定義を再考するきっかけとなるかもしれない．

まず，今回の発見に至るまでの経緯を述べる．APMV（*Acanthamoeba polyphaga* mimivirus）は，現在確認されているウイルスの中で最大径のウイルス種である．その直径は約400 nmであり，マイコプラズマと同等のサイズということからも，その巨大さが窺い知れる．そもそもの発端は，1992年，イングランドで流行した肺炎にある．その原因究明のため，同国各所からサンプルが集められた．その際，ブラッドフォードの冷却塔に生息していたアメーバ中から，グラム陰性菌らしきものが確認された[1]．原核生物の同定に頻用されるrDNA sequencingでもその病原体の正体は明らかにされないまま，11年の月日が流れた．そして2003年，詳細な解析の結果，その細菌らしきものの正体は，なんとウイルスであることが判明したのである[3]．さらにその翌年（2004年），ゲノム解析によって，そのウイルスは1.2 Mbもの直鎖DNAをゲノムとして有していること，1262個の翻訳領域（open reading flame，ORF）を有していることが明らかとなった[5]．そのウイルス粒子の巨大さ，そして保有するゲノムの大きさから，「細菌を模倣しているウイルス（*mi*micking *mi*crobes *virus*）」として，「ミミウイルス（mimivirus）」と名づけられた[2]．

さて，紹介論文[4]のノイエスはふたつある．ひとつめは，APMVの新種「ママウイルス（mamavirus）」が，フランス・パリの冷却塔から新たに見つかったこと．ウイルス粒子のサイズがミミウイルスよりも一回り大きいことから，ママウイルスの発見は，最大のウイルスを更新するものである．そして，ふたつめは，ママウイルスに感染したそのアメーバの中から，まったく別のウイルス様粒子が見つかったことにある．「スプートニク（Sputnik）」というソ連が打ち上げた世界初の無人人工衛星の名を冠されたこのウイルスの直径は50 nmで，約18 kbの環状DNAをゲノムとして持っている．そして，興味深いことに，ママウイルス粒子の中にも，このスプートニク粒子が確認されたのである．さらにスプートニクは，mamavirus factoryと称される，ママウイルス由来のタンパク質から構成されていると考えられる細胞内器官を利用して複製することが，蛍光抗体法による解析から推察された．スプートニクのこの複製スタイルが，細菌におけるバクテリオファージ（bacteriophage）のそれと類似していることから，筆者らは，「スプートニクは，『別のウイルス（ママウイルス）に感染するウイルス』と言えるのではないか」，と述べた上で，バクテリオファージにちなんで，“virophage”という概念を提唱している．

APMV（ミミウイルスとママウイルス）は分類上，nucleocytoplasmic large DNA viruses（NCLDVs）に属しているものの，これまでの「ウイルス」という概念からは遠くかけ離れた特徴をいくつか有している．まず，その粒子の形状である．約400 nmという大きさだけでも驚きだが，さらにこのウイルスは，エンベロープ膜の代わりに，原繊維（fibril）というもので覆われている．また，APMVは1.2 Mbという非常に大きなゲノムを有している．これは，梅毒の原因となる真正細菌 *T. pallidum* と同等のゲノムサイズであることからも[1]，その異常な大きさが推察できる．そして，その茫漠なゲノムの中に，1262個もの多種多彩なORFを有していることが確認されている[5]．その

連絡先
〒606-8507
京都大学ウイルス研究所ウイルス病態研究領域
TEL：075-751-4813
FAX：075-751-4812
E-mail：ykoyanag@virus.kyoto-u.ac.jp

ORFの約70%はその塩基配列から機能が予測されており，APMVと同じNCLDVsに分類されるボックスウイルス，種々の細菌類，さらにはほ乳類と相同性のあるORFを複数保有していることが予測されている[5]．そして，特筆すべきは，それらの予測ORFが，tRNA合成酵素，DNA修復酵素，翻訳関連タンパク質，シャペロン分子などもコードしていることである．これはすなわち，リボソーム以外のタンパク質翻訳に必要な分子はほとんど自前で用意していると言っても過言ではない．このことから，APMVは，「リボソームを持たない生物」とも表現できるかもしれない（実際筆者らは，ある総説[6]において，APMVを「キャプシドに包まれた生物と分類すべきである」とも提唱している）．

とは言え，APMVの複製は完全にアメーバに従属しており，これまでの定義からすればやはり，APMVは「ウイルス」の範疇を出ない．さらに，スプートニクも，ママウイルスの複製に従属しているとは言え，ママウイルスはもとよりアメーバなしでは複製することができない．これらのことをふまえると，現在の定義によれば，スプートニクはあくまで，サテライトウイルス（ヘルパーウイルス）に分類されることとなる．

しかしながらウイルスとは，ひとくちに「ウイルス」とカテゴライズされているものの，その形態はもとより，複製様式は枚挙に暇がない．APMVという，これまでの一般的なウイルスのイメージを覆すような巨大ウイルスの発見と，それに「寄生」するかのような小さなサテライトウイルスの発見が，「ウイルス」といういささか広範すぎる枠組みを見つめ直すきっかけとなるかもしれない．

引用文献

1）Birtles RJ, Rowbotham TJ, Storey C, Marrie TJ, Raoult D.: Chlamydia-like obligate parasite of free-living amoebae. Lancet 349, 925-926, 1997.
2）Koonin E V. Virology: Gulliver among the Lilliputians.: Curr Biol 15, R167-169, 2005.
3）La Scola B, Audic S, Robert C, Jungang L, de Lamballerie X, Drancourt M, Birtles R, Claverie J M, Raoult D.: A giant virus in amoebae. Science 299, 2033, 2003.
4）La Scola B, Desnues C, Pagnier I, Robert C, Barrassi L, Fournous G, Merchat M, Suzan-Monti M, Forterre P, Koonin E, Raoult D.: The virophage as a unique parasite of the giant mimivirus. Nature 455, 100-104, 2008.
5）Raoult D, Audic S, Robert C, Abergel C, Renesto P, Ogata H, La Scola B, Suzan M, Claverie J M.: The 1.2-megabase genome sequence of Mimivirus. Science 306, 1344-1350, 2004.
6）Raoult D, Forterre P.: Redefining viruses: lessons from Mimivirus. Nat Rev Microbiol 6, 315-319, 2008.

Journal of Neuroscience Research 87:307–317 (2009)

Evaluation of Human Fetal Neural Stem/Progenitor Cells as a Source for Cell Replacement Therapy for Neurological Disorders: Properties and Tumorigenicity After Long-Term In Vitro Maintenance

Daisuke Ogawa,[1,2] Yohei Okada,[1,3] Masaya Nakamura,[4] Yonehiro Kanemura,[5] Hirotaka James Okano,[1] Yumi Matsuzaki,[1] Takuya Shimazaki,[1] Mamoru Ito,[6] Eiji Ikeda,[7] Takashi Tamiya,[2] Seigo Nagao,[2] and Hideyuki Okano[1]*

[1]Department of Physiology, School of Medicine, Keio University, Tokyo, Japan
[2]Department of Neurological Surgery, Faculty of Medicine, Kagawa University, Kagawa, Japan
[3]Department of Neurology, Graduate School of Medicine, Nagoya University, Nagoya, Japan
[4]Department of Orthopedic Surgery, School of Medicine, Keio University, Tokyo, Japan
[5]Institute for Clinical Research, Osaka National Hospital, National Hospital Organization, Osaka, Japan
[6]Central Institute for Experimental Animals, Tokyo, Japan
[7]Department of Pathology, School of Medicine, Keio University, Tokyo, Japan

It is expected that human neural stem/progenitor cells (hNS/PCs) will some day be used in cell replacement therapies. However, their availability is limited because of ethical issues, so they have to be expanded to obtain sufficient amounts for clinical application. Moreover, in-vitro-maintained hNS/PCs may have a potential for tumorigenicity that could be manifested after transplantation in vivo. In the present study, we demonstrate the in vitro and in vivo properties of long-term-expanded hNS/PCs, including a 6-month bioluminescence imaging (BLI) study of their in vivo tumorigenicity. hNS/PCs cultured for approximately 250 days in vitro (hNS/PCs-250) exhibited a higher growth rate and greater neurogenic potential than those cultured for approximately 500 days in vitro (hNS/PCs-500), which showed greater gliogenic potential. In vivo, both hNS/PCs-250 and -500 differentiated into neurons and astrocytes 4 weeks after being transplanted into the striatum of immunodeficient mice, and hNS/PCs-250 exhibited better survival than hNS/PCs-500 at this time point. We also found that the grafted hNS/PCs-250 survived stably and differentiated properly into neurons and astrocytes even 6 months after the surgery. Moreover, during the 6-month observation period by BLI, we did not detect any evidence of rapid tumorigenic growth of the grafted hNS/PCs, and neither PCNA/Ki67-positive proliferating cells nor significant malignant invasive features were detected histologically. These findings support the idea that hNS/PCs may represent a nontumorigenic, safe, and appropriate cell source for regenerative therapies for neurological disorders. © 2008 Wiley-Liss, Inc.

Key words: neural stem cell; in vivo optical imaging; long-term cultures; long-term engraftment; immunodeficient mouse

Recent progress in stem cell biology has greatly raised the expectation that cell replacement therapies may be developed for a variety of neurological disorders, such as spinal cord injury and neurodegenerative diseases, by using human fetal neural stem/progenitor cells (hNS/PCs) (Reynolds and Weiss, 1992; Svendsen et al., 1998; Carpenter et al., 1999; Uchida et al., 2000; Caldwell et al., 2001; Keyoung et al., 2001; Okano, 2002; Jeong et al., 2003; McBride et al., 2004; Cummings et al., 2005; Iwanami et al., 2005). However, the limited availability of human fetal tissues for ethical reasons makes it difficult to obtain large amounts of hNS/PCs. Therefore, for clinical applications, it is important to be able to expand hNS/PCs in vitro in a manner that maintains their multipotency and ability to self-renew.

Additional Supporting Information may be found in the online version of this article.

Contract grant sponsor: Leading Project for Realization of Regenerative Medicine from the Ministry of Education, Culture, Sports, Science and Technology (MEXT) of Japan; Contract grant sponsor: Japan Science and Technology Agency (SORST); Contract grant sponsor: Ministry of Health, Labor, and Welfare (to H.O.); Contract grant sponsor: Research Fellowships for Young Scientists from the Japan Society for the Promotion of Science (to Y.O.); Contract grant sponsor: Grant-in-Aid for 21st Century COE Program from the MEXT (to Keio University).

*Correspondence to: Hideyuki Okano, MD, PhD, Department of Physiology, Keio University School of Medicine, 35 Shinanomachi, Shinjuku-ku, Tokyo 160-8582, Japan. E-mail: hidokano@sc.itc.keio.ac.jp

Received 29 March 2008; Revised 12 June 2008; Accepted 13 June 2008

Published online 28 October 2008 in Wiley InterScience (www.interscience.wiley.com). DOI: 10.1002/jnr.21843

In addition, because of their low proliferation rate, it takes a long time for hNS/PCs to be expanded from a small number of cells to a sufficient population to use in cell replacement therapies. However, previous in vitro studies showed that subjecting hNS/PCs to multiple passages for up to 300 days in vitro (DIV) reduces their growth rate and alters their neurogenic potential (Caldwell et al., 2001; Kanemura et al., 2002; Piao et al., 2006; Wright et al., 2006; Anderson et al., 2007). Neither the proliferative and differentiation properties nor the in vivo dynamics have been reported for hNS/PCs cultured for longer than 300 DIV. Moreover, the long-term in vivo tumorigenicity of grafted hNS/PCs has never been described and is still uncertain.

Here we examined, both in vitro and in vivo, the differentiation and growth properties of hNS/PCs maintained for approximately 250 DIV (hNS/PCs-250) compared with hNS/PCs maintained for a longer period, approximately 500 DIV (hNS/PCs-500). Furthermore, we established a system for evaluating the in vivo tumorigenicity of hNS/PCs, by transplanting them into the striatum of immunodeficient mice and continuously monitoring the transplanted cells by bioluminescence imaging (BLI) in combination with conventional histology. With this system, we successfully monitored grafted cells for approximately 6 months, to evaluate the tumorigenicity of hNS/PCs as a source for cell replacement therapies.

MATERIALS AND METHODS

Cell Culture

Approval to use human fetal neural tissues and neurosphere cultures was obtained from the ethical committees of Keio University and Osaka National Hospital. Tissue procurement procedures were in accordance with the Declaration of Helsinki and in agreement with the ethical guidelines of the Japan Society of Obstetrics and Gynecology and with the ethical guidelines of the Network of European CNS Transplantation and Restoration (NECTAR). Forebrain tissues from a human fetus (8 weeks gestational age) were obtained from a legal abortion carried out at the Osaka National Hospital, with written informed consent obtained from the donor.

hNS/PCs were cultured using the neurosphere method (Reynolds and Weiss, 1992; Svendsen et al., 1998; Keyoung et al., 2001; Kanemura et al., 2002). The growth medium was a defined DMEM/F-12 (1:1)-based medium (Sigma, St. Louis, MO) supplemented with human recombinant (hr-) epidermal growth factor (20 ng/ml; PeproTech EC Inc., London, United Kingdom), hr-fibroblast growth factor 2 (20 ng/ml; PeproTech EC Inc.), hr-leukemia inhibitory factor (10 ng/ml; Chemicon, Temecula, CA), heparin (5 1g/ml; Sigma), B27 supplement (Invitrogen, Carlsbad, CA), and L-glutamine (200 mM; Invitrogen). Half of the culture medium was replaced with fresh growth medium every week. Neurospheres were passaged every 14 days by dissociating them into single cells using TrypLE select (Invitrogen). Viable cells (2 3 10^6 cells/15 ml) were seeded into 50% fresh growth medium plus 50% neurosphere-conditioned medium in uncoated T75 culture flasks and incubated at 378C in 5% CO_2-95% air. hNS/PCs-250 represent neurospheres passaged 20–25 times; 244–314 DIV; mean 287.3 6 24.2 DIV. hNS/PCs-500 represent neurospheres passaged 36–40 times; 476–526 DIV; mean 503.0 6 18.8 DIV (mean 6 SD).

To induce differentiation, the dissociated hNS/PCs were plated on poly-L-lysine (PLL)-coated coverslips and cultured in the DMEM/F-12/B27 without growth factors (Svendsen et al., 1998; Carpenter et al., 1999; Vescovi et al., 1999) for 7 days. On day 7, the cells were fixed in 4% paraformaldehyde (PFA) for 15 min and processed for immunocytochemical analysis.

Growth Assay

To measure the number of viable cells, the total ATP content was measured by ATP assay using the CellTiter-Glo Luminescent Cell Viability Assay (Promega, Madison, WI; Crouch et al., 1993; Petty et al., 1995). Single-cell suspensions were prepared from neurospheres by enzymatic dissociation with TrypLE select. The number of viable cells in the single-cell suspensions was determined by cell counting using trypan blue dye exclusion. To create a standard curve, 100-11 single-cell suspensions of known densities (1 3 10^5, 2 3 10^5, 4 3 10^5, and 8 3 10^5 cells/ml) were subjected to the ATP assay.

To assay the growth of hNS/PCs-250 and -500, single-cell suspensions from each neurosphere were plated in a 96-well plate (5 3 10^3 cells/100 11). The cell number plated in each well on day 0 was equalized according to the ATP measurement, and the subsequent measurements were normalized to the value on day 0 (day 0 5 1, relative growth rate to day 0). Fresh medium (20 11) was added every 4 days. The ATP assay was performed on days 0 (3 hr after plating), 2, 4, 7, and 11, by adding 100 11 of CellTiter-Glo Reagent to each well adjusted to 100 11 in advance. The luminescence signals were measured by a chemiluminescence detection system (Centro LB960; Berthold Technologies, Bad Wildbad, Germany).

Flow Cytometry

For cell-cycle analysis, the dissociated cells (1 3 10^6 cells) were incubated in 1 ml of hypotonic propidium iodide (PI) solution (1 mg/ml PI, 0.1% citric acid, 0.2% NP-40, 10 mg/ml RNaseA) (Deitch et al., 1982) for 30 min at 48C, followed by a 15-min incubation at 378C to digest the RNA. The fluorescent intensity of the PI was then measured by flow cytometry.

For the cell-surface marker analysis and viability assay, the dissociated cells were incubated in fresh medium at 378C for 1 hr to recover the cell-surface antigens. The cells (1 3 10^7 cells) were suspended in 100 11 Hanks' balanced salt solution (HBSS) and incubated on ice for 30 min with allo phyco cyanin (APC)-conjugated anti-CD133 (Miltenyi Biotec, Tokyo, Japan) and phycoerythrin (PE)-conjugated anti-CD24 (BD Biosciences, Franklin Lakes, NJ), or fluorescvein isothiocyanate (FITC)-conjugated annexin V (BD Biosciences) to detect apoptosis. The cells were washed, resuspended in HBSS containing 1 1g/ml PI, and analyzed by FACS Caliber (BD Biosciences).

Virus Transduction and Bioluminescence Imaging

For the live monitoring of transplanted cells in vivo, we applied bioluminescent imaging (BLI), which has been described previously (Miyoshi et al., 1998; Okada et al., 2005). Human neurospheres and control U87MG cells were transduced by a lentivirus containing the click beetle red luciferase (CBRluc) coding sequence and Venus bicistronic reporter gene connected by an internal ribosomal entry site (IRES) (EF1a-CBRluc-IRES-Venus) (Supp. Info. Fig. 1A). The Venus-positive cells were then collected by a fluorescence-activated cell sorter (FACS) to establish cell lines that stably expressed Venus and CBRluc, as described previously (Masuda et al., 2007) (briefly summarized in Supp. Info. Fig. 1B). We confirmed that the photon counts from these CBRluc-labeled cells were directly proportional to the cell numbers plated in vitro (total cell numbers ranging from 10^2 to 10^6 cells/dish, Supp. Info. Fig. 1C,D). Moreover, the relative number of cells integrated into the host animals after transplantation could be estimated by measuring the photon counts from live animals after an intraperitoneal injection of D-luciferin. We also confirmed that the transduction with the lentivirus did not affect the proliferation or differentiation of hNS/PCs or the survival of the grafted animals (Supp. Info. Fig. 1E,F). A Xenogen-IVIS 100 cooled CCD optical macroscopic imaging system (Caliper Life Sciences, Hopkinton, MA) was used for BLI. All the images were analyzed with Igor (WaveMetrics, Lake Oswego, OR) and Living Image software (Caliper Life Sciences), and the optical signal intensity was expressed as photon counts, in units of photons per second. Each image was displayed as a pseudocolor photon count image superimposed on a gray-scale anatomic image. To quantify the measured luminescence, we defined a specific region of interest (ROI) that covered the area in and around the implanted cells. We used the same ROI for all the animals at all time points to ensure uniform data collection.

Transplantation

All the animal experiments were conducted according to the Guidelines for the Care and Use of Laboratory Animals of the Keio University School of Medicine. Mice were anesthetized and received implants of partially dissociated human neurospheres (2 3 10^6 cells in 4 1l of PBS) stereotactically into the right striatum (2 mm lateral and 1 mm anterior to bregma; depth 3 mm from dura). We used immunodeficient mice to avoid immunological rejection resulting from the xenograft. For short-term analyses of up to 4 weeks, we used NOD/SCID/γ_c^{null} (NOG) mice (Central Institute for Experimental Animals, Kanagawa, Japan), which are deficient for the common receptor gamma chain on the severe combined immunodeficiency (NOD/SCID) background (Ito et al., 2002) (n 5 5 for hNS/PCs-250, n 5 4 for hNS/PCs-500, n 5 4 for U87MG). NOD/SCID mice (Charles River, Tokyo, Japan) were used for long-term observation of up to 6 months (n 5 4 for hNS/PC-250, n 5 4 for hNS/PCs-500, n 5 4 for U87MG).

Animals were anesthetized and transcardially perfused with 4% PFA at 4 weeks (1 month), 12 weeks (3 months), and 24 weeks (6 months) after transplantation. The whole brain was removed and postfixed for 8 hr in 4% paraformaldehyde (PFA), soaked overnight in 15% followed by 30% sucrose, and embedded in OCT compound. Coronal sections 14 1m thick were made with a Cryostat (Leica, Wetzlar, Germany) and processed for immunohistochemical analysis.

Immunohistochemistry and Immunocytochemistry

For immunofluorescence analyses, cultured cells or tissue sections were incubated with the following primary antibodies at 48C overnight: anti-human Nestin (1:30,000, rabbit polyclonal) (Nakamura et al., 2003), anti-TuJ-1 (1:500, mouse IgG2b monoclonal) (Sigma), antiglial fiibrillary acidic protein (GFAP) (1:3,000, rabbit polyclonal, Sigma), anti-green fluorescent protein (GFP; 1:25,000, mouse IgG2a, mFX72; a gift from Dr. S. Mitani), anti-Ki67 (1:500, Rb polyclonal IgG) (Novocastra Laboratories, Newcastle Upon Tyne, United Kingdom), antiproliferating cell nuclear antigen (PCNA) (1:1,000; Rb polyclonal IgG) (Oncogene, Boston MA), and anti-human nuclei (1:100, mouse monoclonal IgG1) (Chemicon). After three washes, the samples were incubated with Alexa 488-, 555-, or 647-conjugated secondary antibodies (Invitrogen) for 2 hr at room temperature. Images were obtained by microscopy (Apotome; Carl Zeiss) or confocal laser scanning microscopy (LSM510; Carl Zeiss).

The quantification of different phenotypes in vitro was accomplished by counting the immunolabeled cells on each coverslip. Five separate, randomly chosen fields on each coverslip were counted using a 3 20 objective. The numbers of Nestin-, TuJ-1-, and GFAP-immunoreactive cells are presented as the percentage of total cells, which were stained by Hoechst 33258.

To quantify the Ki67-, PCNA-, and TUNEL-positive cells in tissue sections, the number of immunoreactive cells that were also positively stained by anti-human nuclei were counted in more than five randomly selected fields in each section. These data are presented as the percentage of total cells stained by human antinuclear antigen. Hematoxylin-eosin (HE) staining and HRP-DAB staining were carried out according to standard histological protocols.

Statistical Analysis

Statistical analyses were performed with Student's t-test and Dunn's test. Values are presented as the mean 6 SEM. Significance was accepted at $P < 0.05$.

RESULTS

hNS/PCs Cultured for Long Periods Lost Their Proliferation Ability In Vitro

We first compared the properties of hNS/PCs-250 with those of hNS/PCs-500 in vitro, including the growth rate and differentiation potentials. By ATP assay (Kanemura et al., 2002), hNS/PCs-250 exhibited a significantly higher growth rate than did hNS/PCs-500 (Fig. 1A). Cell-cycle analysis by PI staining showed that the proportion of dividing cells in S/G2/M was 20.5% 6 1.2% for hNS/PCs-250, which was significantly higher than that for hNS/PCs-500 (12.7% 6 0.2%) (n 5 3, $P < 0.01$; Fig. 1B). However, there was no

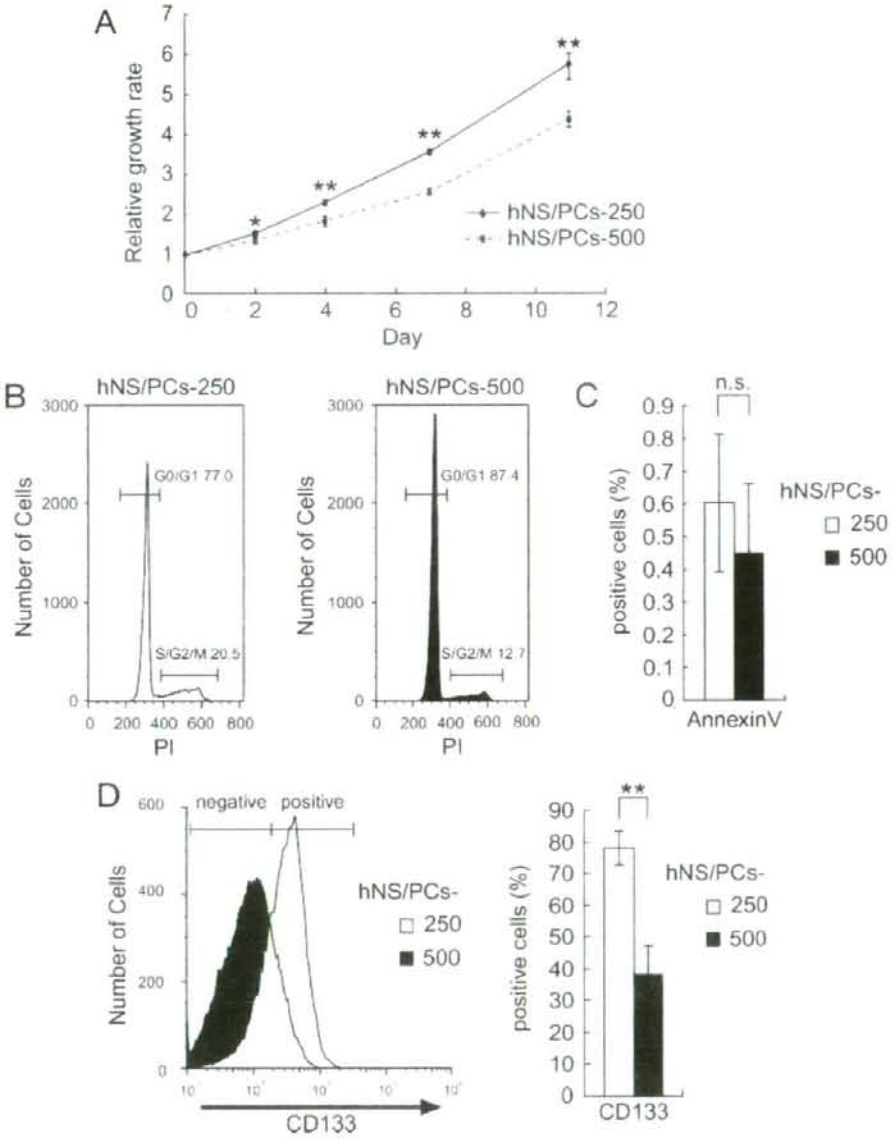

Fig. 1. Comparison of the in vitro properties of hNS/PCs-250 and -500. A: Growth rate of hNS/PCs-250 and -500 examined by ATP assay. hNS/PCs-250 exhibited a significantly higher growth rate than did hNS/PCs-500 during 11 days of culture. B: Cell-cycle analysis by PI staining. The proportion of dividing cells in S/G2/M was significantly higher in hNS/PCs-250 than in -500 ($P < 0.01$). C: Analysis of apoptotic cells by annexin V staining. No significant difference in the proportions of annexin V-positive cells was observed between hNS/PCs-250 and -500. n.s., Not significant ($P > 0.05$). D: Expression of CD133, a marker for undifferentiated hNS/PCs, in hNS/PCs-250 and -500 analyzed by flow cytometry. hNS/PCs-250 contained significantly more $CD133^{+}$ cells than did -500. All data are presented as the mean ± SEM (n = 3). *$P < 0.05$; **$P < 0.01$.

significant difference in the proportion of apoptotic cells stained with annexin V between hNS/PCs-250 and -500 (Fig. 1C). These results suggest that the difference in the in vitro growth rate between hNS/PCs-250 and -500 by ATP assay might be attributable to the presence of a differing proportion of proliferating cells, but not of apoptotic cells.

We speculated, based on these results, that there might be a difference in the proportion of undifferentiated hNS/PCs in the neurospheres of hNS/PCs-250 and -500. Therefore, we examined dissociated neurospheres for the expression of cell-type-specific surface markers by flow cytometry. The results indicated that the proportion of $CD133^{+}$ cells, which are known to represent an enriched population of neurosphere-initiating cells (Uchida et al., 2000; Barraud et al., 2007; Panchision et al., 2007), in hNS/PCs-250 was approximately twice that in hNS/PCs-500 (77.9% 6 5.2% and 38.2% 6 8.9% in hNS/PCs-250 and -500, respectively, $P < 0.01$; Fig. 1D), suggesting that the $CD133^{+}$ hNS/PCs in neurospheres may contribute to the higher growth rate seen in hNS/PCs-250 vs. hNS/PCs-500.

hNS/PCs-250 Generated Relatively More Neurons, Whereas hNS/PCs-500 Generated More Astrocytes

We next allowed hNS/PCs-250 and -500 to differentiate on PLL-coated coverglasses without growth factors for 7 days and examined their phenotypes by immunocytochemistry. There was no significant difference in the percentage of Nestin-positive cells between hNS/PCs-250 and -500 (Fig. 2A,B). However, whereas more than 50% of the hNS/PCs-250 differentiated into TuJ-1-positive neurons (54.3% 6 5.5% and 17.6% 6 3.0% in hNS/PCs-250 and -500, respectively, n 5 3, P < 0.01), more than 70% of the hNS/PCs-500 differentiated into GFAP-positive astrocytes (23.6% 6 14.7% and 73.5% 6 6.6% in hNS/PCs-250 and -500, respectively, n 5 3, $P < 0.05$). As previously reported, neither hNS/PCs-250 nor hNS/PCs-500 differentiated into CNPase-positive oligodendrocytes in vitro under the same conditions (Iwanami et al., 2005) (data not shown). Consistently with these findings, flow cytometric analyses showed that hNS/PCs-250 contained a greater proportion of $CD24^{+}$ cells, which are proposed to include the cells committed to neuronal lineages (Calaora et al., 1996; Shewan et al., 1996; Doetsch et al., 1999; Nieoullon et al., 2005; Panchision et al., 2007), than did hNS/PCs-500 (73.2% 6 5.4% and 56.1% 6 5.4% in hNS/PCs-250 and -500, respectively, n 5 3, $P < 0.05$; Fig. 2C). Interestingly, most and some of the $CD24^{+}$ cells in the hNS/PCs-250 and -500 were also positive for CD133 (82.2% and 41.8%, respectively; Fig. 2D). Therefore, we also analyzed the $CD133^{2}$ populations and found that the proportion of $CD133^{2}$ cells that were $CD24^{+}$, possibly those representing neuronal progenitors and postmitotic neurons, tended to be higher in the hNS/PCs-250 than in the hNS/PCs-500, although the difference was not statistically significant (61.1% and 51.6% in hNS/PCs-250 and -500, respectively, P 5 0.06; Fig. 2D). Taken together, these findings suggest that hNS/PCs-250 may contain more neurogenic progenitors than do the hNS/PCs-500, which contain more gliogenic progenitors.

hNS/PCs-250 Exhibited Better Survival After Transplantation Into the Striatum of NOG Mice Than Did hNS/PCs-500 by In Vivo Imaging

To assess the survival and differentiation potentials of hNS/PCs in vivo, we stereotactically transplanted hNS/PCs-250, hNS/PCs-500, or U87MG cells, a human glioblastoma cell line, into the right striatum of the intact mouse brain. To avoid immunological rejection of the grafted cells, we used NOG mice (Ito et al., 2002), which are deficient for the interleukin-2 receptor common g chains under the background of severe combined immunodeficiency (NOD/SCID) mice (Shultz et al., 1995).

After transplantation, we observed the survival and growth of the grafted hNS/PCs and U87MG cells for up to 4 weeks (n 5 4 each). For the live monitoring of transplanted cells in vivo, we labeled the hNS/PCs and U87MG with a lentivirus containing the coding sequence for CBRluc and a Venus reporter gene (EF1a-CBRluc-IRES-Venus) (Supp. Info. Fig. 1A) and applied BLI (Okada et al., 2005). The BLI results revealed that the surviving grafted hNS/PCs-250 and -500 decreased sharply, to approximately 20–40% of their original levels 1 week after the transplantation and were maintained thereafter. Four weeks after the transplantation, hNS/PCs-250 showed significantly better survival than did hNS/PCs-500 (12.7% 6 2.4% and 3.8% 6 1.0% of the initial photon counts in hNS/PCs-250 and -500, respectively, n 5 4, $P < 0.01$; Fig. 3A,B). In contrast, the U87MG glioblastoma cells showed logarithmic growth during the 4-week observation period.

Immunohistochemical analyses revealed that both hNS/PCs-250 and hNS/PCs-500 had differentiated into TuJ1-positive neurons and GFAP-positive astrocytes 4 weeks after the transplantation (Fig. 4A). Nestin-positive neural progenitors were also observed in both the hNS/PCs-250 and the hNS/PCs-500 grafts. hNS/PCs-250 contained significantly more Ki67- and PCNA-positive cells than did hNS/PCs-500 (Ki67: 5.1% 6 0.8% and 3.1% 6 0.3%, $P < 0.05$; PCNA: 5.8% 6 0.2% and 4.4% 6 0.3%, in hNS/PCs-250 and -500, respectively, n 5 3, $P < 0.01$; Fig. 4B,C). The percentage of TUNEL-positive apoptotic cells was not significantly different between hNS/PCs-250 and hNS/PCs-500 (0.26% 6 0.05% and 0.37% 6 0.14%, respectively, n 5 3; Fig. 4D,E).

Grafted Neurospheres Survived and Differentiated Into Neurons and Astrocytes In Vivo but Did Not Show Tumorigenicity Even 6 Months After Transplantation

Finally, we evaluated the long-term survival of hNS/PCs and investigated their safety as a cell source

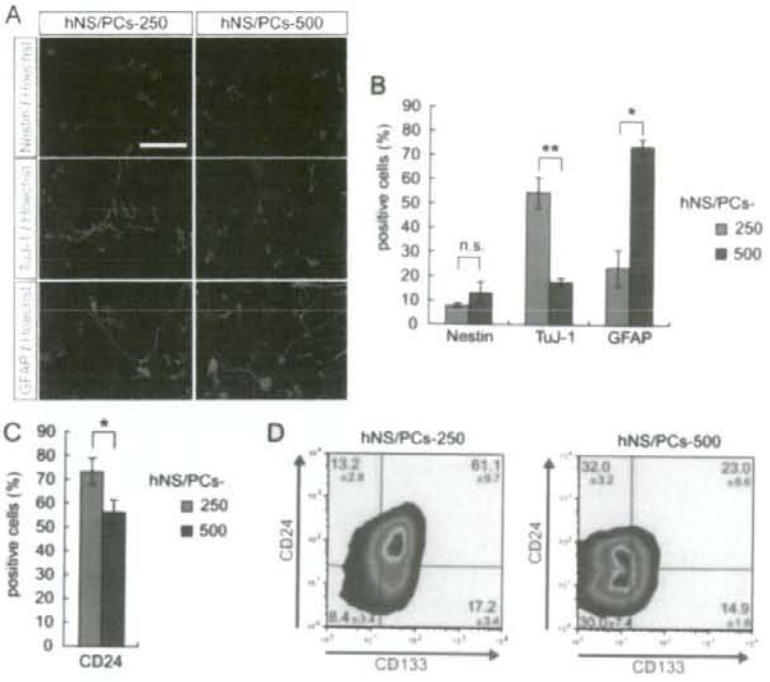

Fig. 2. Altered differentiation potentials between hNS/PCs-250 and -500. A: Immunocytochemical analysis of differentiated hNS/PCs for markers of neural progenitors (Nestin), neurons (TuJ-1), and astrocytes (GFAP). Quantitative analysis is shown in B. Only approximately 10% of the cells in both hNS/PCs-250 and -500 remained positive for Nestin. hNS/PCs-250 differentiated into significantly more TuJ-1-positive neurons than did hNS/PCs-500, whereas hNS/PCs-500 differentiated into significantly more GFAP-positive astrocytes than did hNS/PCs-250. C: Flow cytometric analysis of CD24, which is expressed in populations that include neuronal progenitors and postmitotic neurons. Consistent with the results in B, hNS/PCs-250 contained significantly more CD24-positive cells than did hNS/PCs-500. D: Coexpression of CD133 and CD24 by flow cytometric analysis. Consistently with the results in Figures 1 and 2B, hNS/PCs-250 contained significantly more $CD133^{1}$ cells and $CD24^{1}$ cells than did hNS/PCs-500; n 5 3; means 6 SEM. *P < 0.05; **P < 0.01; n.s., not significant (P > 0.05). Scale bar 5 50 1m.

for transplantation therapy. For long-term observation, we used NOD/SCID mice, which are resistant to stress and infection and therefore show better survival than NOG mice. The results of the short-term experiment revealed that hNS/PCs-500 showed a lower proliferation ability than hNS/PCs-250 in vivo by Ki67 or PCNA immunostaining and a poor survival rate by BLI (only 3.8% 1 month after transplantation even in NOG mice) (Fig. 3A). Thus, for this long-term experiment, we monitored the in vivo tumorigenicity of only the hNS/PCs-250, as the better cell source for cell replacement therapy.

We transplanted hNS/PCs-250 into the right striatum of NOD/SCID mice and observed the survival of the grafted hNS/PCs by BLI for 6 months. The photon count of the luminescence generated by the surviving hNS/PCs was reduced to 12.8% 6 11.0% of the initial photon count at 8 weeks and thereafter maintained its signal for 6 months (10.0% 6 14.0%, n 5 4; Fig. 5A). Notably, no rapid tumorigenic increase of the grafted hNS/PCs was observed within the 6 months following the transplantation. In contrast, control U87MG cells grew rapidly, showing a 419% increase in photon count 4 weeks after transplantation. Among the U87MG-transplanted mice, 75% (three of four) died by 5 weeks and the rest by 6 weeks after transplantation.

To examine the phenotype of the surviving cells derived from the transplanted hNS/PCs, we performed immunohistochemical analyses. Consistent with the findings of BLI, surviving Venus-positive cells were detected 3 months after transplantation (Fig. 5B). Most of them resided at the transplantation site for the entire 6 months and differentiated into TuJ-1-positive neurons and GFAP-positive astrocytes (Fig. 5C). In addition, Nestin-positive neural progenitors persisted even 6 months after the transplantation. However, the grafted hNS/PCs 6 months after transplantation in the long-term animals appeared to have larger nuclei and

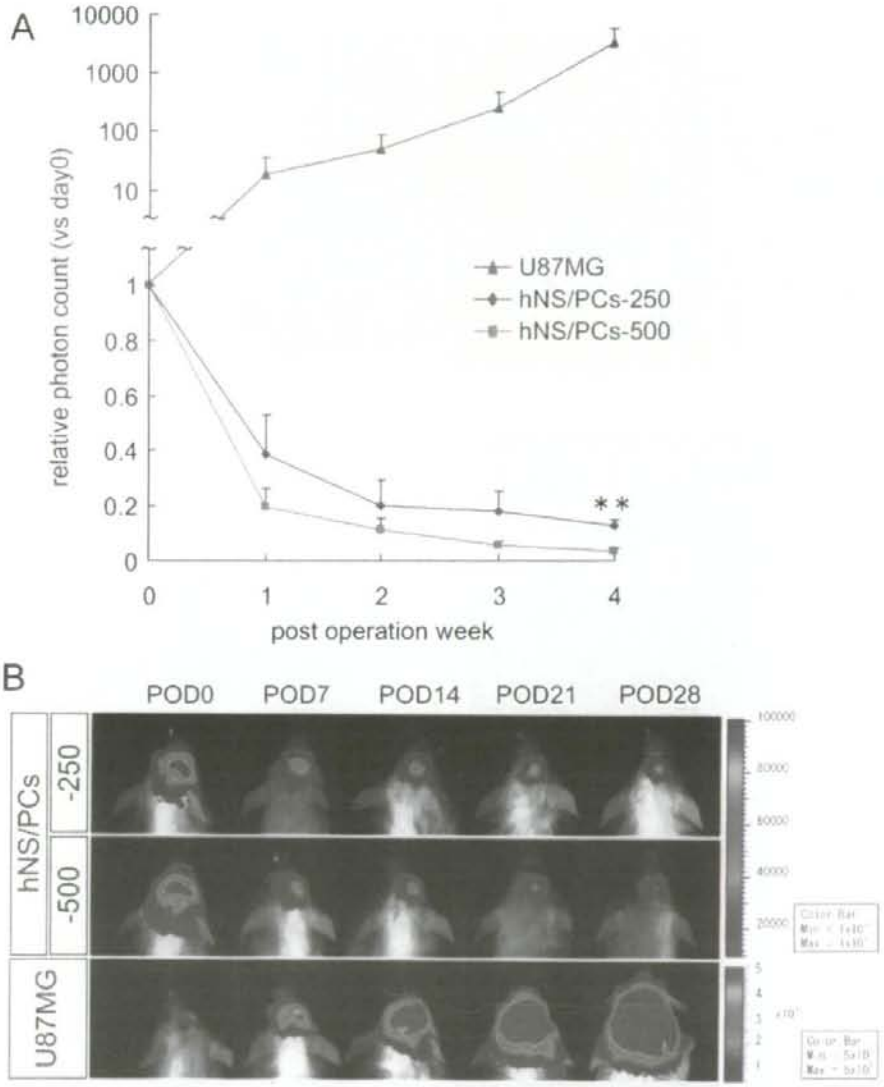

Fig. 3. Bioluminescence imaging of hNS/PCs-250 and -500 transplanted into NOG mice for up to 4 weeks. A: hNS/PCs-250, -500, and human glioblastoma cells (U87MG) were transplanted into the right striatum of NOG mice and observed by BLI for up to 4 weeks. hNS/PCs-250 exhibited significantly better survival and growth than did hNS/PCs-500 4 weeks after transplantation (n 5 4; means 6 SEM). **P < 0.01. B: Representative BLI images of the treated mice.

lower cell densities than those observed 4 weeks after transplantation in the short-term animals (Fig. 5D). Importantly, we did not find any proliferating cells labeled by Ki67 or PCNA 6 months after transplantation (Fig. 5E) nor any obvious evidence of malignant invasive behavior by HE staining (Fig. 5F). Together